Front. Chem. Sci. Eng. 2019, 13(2): 330–339
https://doi.org/10.1007/s11705-019-1803-6

RESEARCH ARTICLE

Multifunctional antimicrobial chlorhexidine polymers by remote plasma assisted vacuum deposition

Ana Mora-Boza[1], Francisco J. Aparicio (✉)[1], María Alcaire[1], Carmen López-Santos[1], Juan P. Espinós[1], Daniel Torres-Lagares[2], Ana Borrás[1], Angel Barranco (✉)[1]

1 Consejo Superior de Investigaciones Científicas. Instituto de Ciencia de Materiales de Sevilla (CSIC-Universidad de Sevilla) c/Américo Vespucio 49, 41092 Sevilla, Spain
2 Facultad de Odontología, Universidad de Sevilla (USE) c/Avicena, 41009 Sevilla, Spain

Abstract Novel antibacterial materials for implants and medical instruments are essential to develop practical strategies to stop the spread of healthcare associated infections. This study presents the synthesis of multifunctional antibacterial nanocoatings on polydimethylsiloxane (PDMS) by remote plasma assisted deposition of sublimated chlorhexidine powders at low pressure and room temperature. The obtained materials present effective antibacterial activity against *Escherichia coli* K12, either by contact killing and antibacterial adhesion or by biocide agents release depending on the synthetic parameters. In addition, these multifunctional coatings allow the endure hydrophilization of the hydrophobic PDMS surface, thereby improving their biocompatibility. Importantly, cell-viability tests conducted on these materials also prove their non-cytotoxicity, opening a way for the integration of this type of functional plasma films in biomedical devices.

Keywords plasma polymers, conformal plasma deposition, chlorhexidine, bactericide, PDMS, biocompatibility

1 Introduction

The outbreak of implants and device-related infections poses serious problems to public health because of its complex and expensive treatment [1–3]. Hospital acquired infectious (HAI) treatments usually involve surgical replacement of the contaminated devices and prolonged antibiotic therapies which are accompanied by long hospitalizations, morbidity and increased mortality [4]. In addition, the rise of antibiotic resistant strains has complicated even more these therapies [1,4–8] standing out the infection by methicilline resistant *Staphylococcus aureus* and the recently discovered silver-resistant gene *silE* due to the widespread usage of silver-based biocides [4,7]. This problem has focused the attention on the urgent development of new biocide surfaces to avoid undesirable microorganism colonizations over implants and medical instruments.

Nowadays, antifouling coating approaches could be classified in biocidal and nonbiocidal surfaces. While the first approach provokes bacteria death through contact killing surfaces or the release of a biocide agent, the second one is also known as a biopassive surface as it impedes the adhesion of microorganisms through physical mechanisms without killing them [1,4–8]. Each mechanism has inherent advantages and limitations, which has motivated intense investigations on the development of bi-functional materials that combine both antibacterial mechanisms [9]. Of course, such coatings should neither have any adverse effect on the host body, fluids, cells and tissues nor impede the normal growth of normal cells over implants. In addition, they should not affect other properties such as the transparency (e.g., contact lenses and catheters) or the flexibility (e.g., vascular grafts) of the medical device.

Antibacterial coatings can be fabricated by a wide range of material fabrication techniques such as electron beam evaporation under vacuum for grafting polymer surfaces, incubation/impregnation/infiltration under vacuum, plasma spraying/resonant infrared, and matrix-assisted pulsed laser evaporation (RIR-MAPLE) [10–13]. However, in recent years the use of vapor and plasma deposition processes to produce nanometer thin coatings has gained more interest for many biomaterial applications due to its numerous advantages [2,5,6,8,13–16].

Received September 1, 2018; accepted December 2, 2018

E-mails: fjaparicio@icmse.csic.es (Aparicio F J),
angelbar@icmse.csic.es (Barranco A)

In this work, we propose a novel straightforward fabrication method of plasma-based biocidal coatings using the well-known antiseptic chlorhexidine (CHX) as precursor for the film deposition. CHX is a bisbiguanide and a broad-spectrum biocide commonly used in liquid solution whose mechanism of action is based on the strong association of biguanide groups to exposed anionic sites on the cell membrane and wall (phospholipids and proteins). Thus, CHX is a contact-based biocide which causes displacements of membranes associated with divalent cations, reducing membrane fluidity significantly and causing bacterial death [3,12,14].

The plasma deposition methodology studied in this work has been developed and applied for the synthesis of photonic films and devices [17–20]. It is named remote plasma assisted vacuum deposition (RPAVD) and is a process that combines a remote plasma discharge with the thermal vacuum deposition of an organic solid on substrates placed in the afterglow. During RPAVD process, a plasma polymer matrix retaining a substantial amount of precursor's functional groups and even a concentration of embedded non-fragmented precursor molecules are grown on the substrates [21,22]. In brief, the main objective of the use of RPAVD process is to fabricate functional organic thin films presenting less cross-linked and more highly functionalized structures than those characteristic of more conventional plasma polymerization processes. Another advantage of RPAVD process is the possibility of using chemical or temperature sensitive substrates for their deposition at room temperature [19].

In this work, we present a study about the development of RPAVD antibacterial coatings on polydimethylsiloxane (PDMS) surfaces. PDMS is an elastomer widely used in the medical field for its numerous suitable properties as elasticity, optical transparency, chemical stability and low cost [23–25]. Nonetheless, the applicability of PDMS and other common silicone based materials is hindered by their intrinsic surface hydrophobicity [23]. This effect in such materials has been related to nonspecific protein adsorption processes that induce coagulation, immunological reactions and other adverse effects for prolonged blood-contacting applications [8,24,25]. In addition, cell adhesion and proliferation are favored on hydrophilic surfaces [3,26,27], which promotes the proper integration under physiological conditions. Due to their low surface-reactivity, the functionalization and hydrophilization of PDMS surfaces by wet chemical routes frequently require multi-step processes eventually involving toxic compounds [28]. To overcome these drawbacks, the surface modification of PDMS by plasma discharges and UV treatments has been intensely investigated but suffers from the fast hydrophobic recovery typically observed in PDMS surfaces after such modifications. This effect has been related to diffusion of hydrophobic low-mass PDMS residues towards the surface and the reorientation of surface polar groups to the polymer bulk [24,28]. It was reported that hydrophobic recovery could be inhibited by treating PDMS surfaces with a chlorine plasma discharge [29]. Besides, additional backing processes in combination with multiple plasma polymer deposition steps proved to be effective way to block the diffusion of PDMS hydrophobic moieties towards the surface [30]. In other studies, a highly cross-linked plasma polymer under-layer is used to prevent the migration of low-weight hydrophobic moieties from the PDMS substrate towards the surface of a hydrophilic plasma coating [31]. To summarize, the main objective of our study is the development of transparent conformal nanocoatings on PDMS presenting bactericidal properties, stable hydrophilicity and biocompatibility for their potential applicability on medical devices.

2 Materials and methods

2.1 Synthesis of CHX nanocoatings by RPAVD

The straightforward fabrication of the biocide nanocoatings was carried out in a microwave electron cyclotron resonance (MW-ECR) plasma reactor set up as detailed elsewhere [14,18,22]. As shown in Fig. 1(a), the experimental system consisted of an ECR plasma reactor with two separated zones for plasma and remote deposition. In the plasma zone, an argon microwave plasma (power 150 W and pressure 10^{-2} mbar) was sustained and confined by a set of magnets. Meanwhile, in the afterglow a thermal cell sublimated the CHX precursor onto substrates placed at the afterglow. Nominal deposition rates (fixed at 0.4 Å/s) and final thicknesses were monitored using a calibrated quartz crystal microbalance and determined after deposition by field emission scanning electron microscopy (FESEM) cross-sectional measurements and by optical methods. The growing rates were slowly and gradually increased at the beginning of each deposition from relatively low rates of 0.01 to 0.4 Å/s and then stabilized at the latter value for the rest of the deposition to increase the cross-linking of the initially deposited films. The system was pumped down to a base pressure of 10^{-6} mbar before and after deposition.

Two different geometrical arrangements were used for the synthesis of the films. In both configurations the sample holder consisted of a grounded metallic mesh placed between the sublimation cell and the plasma zone, at ~7 cm from the discharge and at ~8 cm from the sublimation source. For sample CHX-1 (front configuration in Fig. 1(a)) the substrates faced towards the sublimation source whereas for sample CHX-2 (back configuration in Fig. 1(a)) they faced towards the plasma discharge (see reference 22 for additional technical details). Thus, during deposition, both the incoming organic moieties involved in the synthesis and the growing films were exposed to a softer plasma interaction for CHX-1 samples than that for

CHX-2 samples which were deposited directly exposed to the plasma discharge.

2.2 Materials

CHX (1,1′-hexamethylenebis[5-(4-chlorophenyl)biguanide]) powder purchased from Sigma-Aldrich were sublimated during the deposition process without purification. The RPAVD thin films were deposited on 1 cm × 1 cm pieces of doped and intrinsic silicon (100), gold coated silicon, fused quartz slides and pieces of PDMS foils. PDMS foils were fabricated by mixing the base and the curing agent in 10:1 mass ratio, transferred to a Teflon dish, and cured in a thermal plate for 90 min.

2.3 Experimental characterization methods

X-ray photoelectron spectroscopy (XPS) measurements were performed in a Phoibos 100 DLD X-Ray spectrometer from SPECS. The spectra were recorded in the pass energy constant mode at a value of 50 eV using a Mg K_α source. C1s main signal at 284.6 eV was utilized for the calibration of the binding energies of the spectra.

Fourier transform infrared (FT-IR) spectra were obtained on a JASCO FT/IR-6200 IRT-5000 under vacuum conditions in specular reflectance mode for thin films deposited on gold coated silicon (100) substrates in the range from 4000 to 1000 cm^{-1}. The FT-IR spectra of powdered CHX samples diluted in KBr pellets were recorded in transmission configuration.

Water contact angle (WCA) and diiodomethane contact angle (DCA) were determined with an OCA 20 Dataphysics instrument by depositing macroscopic bi-distilled water (pH 7) and diiodomethane droplets of 1 μL. The average of three measurements per sample was taken as the contact angle value. Surface energy of CHX plasma films was calculated from contact angle values by using the Owens Wendt and Kaelbel approximation [32,33].

High-resolution FESEM images of samples deposited on silicon wafers and PDMS after bacteria incubation were obtained on a Hitachi S4800 microscope at 2 kV as acceleration voltage. Cross sectional views were obtained by cleaving the Si(100) substrate.

Ultraviolet-visible-near infrared (UV-vis-NIR) transmittance spectra of samples deposited on quartz slides fused silica were recorded in a Perkin-Elmer spectrophotometer in the range from 190 to1800 nm.

Antimicrobial activity was determined by Agar diffusion method in contact with *Eschericcia coli* (*E. coli*) K12 strain [34]. The culture was grown overnight in a lysogeny broth (LB) medium at 37°C with stirring. The samples were sterilized for 15 min with short-wavelength ultraviolet light, placed over a bacterial lawn growth in an agar LB plate, and then incubated for 24 h. The results of these tests were based on the visual inspection of the generation of clear zones in the plate that indicates bacterial growth inhibition. After these measurements, bacteria viability over the CHX coated surfaces was visualized using an Olympus BX51 fluorescence microscopy. Fluorescein diacetate (FDA) and propidium iodide (PI) (Sigma-Aldrich) staining solutions were used to determine, respectively, lived and dead bacteria after overnight incubation. FDA stock solution was prepared by dissolving 5 mg FDA in 1 mL of acetone, whereas PI stock solution was used as received. Staining solutions were prepared by diluting PI and FDA stock solutions with fresh phosphate saline buffer (PBS) at volume ratios of 1:1000 and 2:1000, respectively. Samples were incubated with 200 μL of each staining solution for 15 min in dark and then washed three times with fresh PBS. Fluorescence micrographs were taken using two different fluorescent filter cubes (Olympus U-MNIGA3 and U-MWIB3) for each dye and analyzed using the ImageJ software package.

Cell adhesion and viability experiments were performed with an osteoblastic-like cell line (MG-63) obtained from the Center of Scientific Instrumentation of the University of Granada. Thermanox® (TMX) 17 mm diameter discs and TMX discs with poly-lysine coatings were used as positive controls. A cell density of 100.000 cells per well was seeded on the CHX nanocoatings and control samples in complete medium and incubated at 37°C in humidifier air with a 5% of CO_2 in a 24 well-plate. The cells were allowed to reach confluence before seeding on the samples. After 24 h of incubation, the cells were stained with trypan blue (Sigma-Aldrich; Merck Millipore) and their viability was determined with an automatic counter cells (Countess™ Automated Cell Counter, Invitrogen, Carlsbad, California, USA). Trypan blue is a dye used for the counting of living cells by exclusion of said dye. This well-known methodology is based on the fact that live (viable) cells do not capture trypan blue, while dead (non-viable) cells do, providing the percentage of viable cells attached to each surface [35].

3 Results and discussion

3.1 Morphological and optical characterization

Top view measurements by FESEM show a very flat surface of the plasma films, and cross section images used to calculate the thin film thickness (Fig. 1(b)) further confirm the flat surface topography of the nanocoatings. CHX plasma films were also optically transparent (Fig. 1(c)) in the near-UV, visible and near-IR regions of the spectra.

Organic thin films from small functional molecules by RPAVD generally have featureless, homogenous and continuous microstructures and extremely flat surface topographies [19,21,22,36,37]. FESEM (Fig. 1(b)) and atomic force microscopy analyses (data not shown) confirm these microstructural characteristics of the CHX

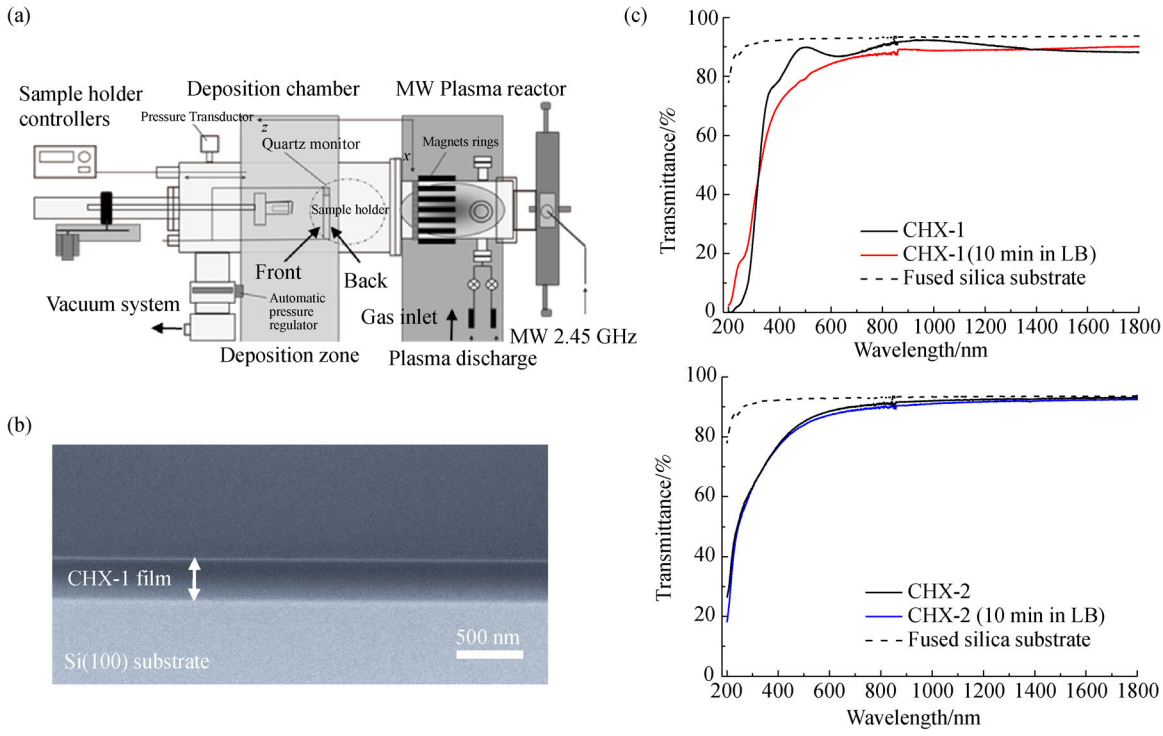

Fig. 1 (a) Experimental set-up; (b) FESEM cross-sectional micrograph of 300-nm-thick CHX-1 film over Si(100); (c) UV-VIS transmission spectra of CHX-1 (top) and CHX-2 (bottom) before and after a LB medium incubation for 10 min

nanocoatings formed by RPAVD.

The lack of light dispersing features is also confirmed by the full transparency of the film in the VIS-NIR region shown in Fig. 1(c). Thus, for wavelengths higher than ~400 nm, the only observed features are the interference fringes due to the refractive index contrast between the RPAVD film and the fused-silica substrate. The transparence of the CHX films is important to assure that the physical appearance of the coated surface is not modified. Besides, the continuous absorption observed in the UV region for wavelength shorter than 300 nm is related to $\pi \rightarrow \pi^*$ transitions involving unsaturated bonds in the plasma polymer [21,22,37].

3.2 Materials characterization

Surface chemical composition of CHX RPAVD films was studied by XPS adjusting the elemental peaks and components according to the literature procedure [14,38–40]. Four photoelectron peaks were observed in the XPS survey of CHX plasma films: O1s, N1s, C1s and Cl2p (Fig. 2(a)). The surface atomic concentrations calculated from these analyses are reported in Table 1. The values indicates a substantial incorporation of oxygen as a consequence of deposition process. Oxygen enrichment of plasma deposited and treated organic material is an extensively reported effect mainly ascribed to the post-deposition reaction between plasma-generated long-lived surface radical and environmental oxygen when the plasma films are exposed to ambient atmosphere. Consequently, this effect is more intense for those samples grown under more severe plasma conditions, i.e., sample CHX-2 (cf. experimental section). The effect of such post-deposition oxidation processes is mainly circumscribed for the surface with a null or negligible oxygen in the bulk of the samples, as it was reported for other plasma polymer films [41,42].

The most remarkable result in Table 1 is that the RPAVD nanocoatings have a high nitrogen concentration, particularly sample CHX-1, the nitrogen concentration of which is similar to that of the CHX molecule. For both CHX nanocoatings, N1s peaks depend on two components: the lowest BE component which is attributed to primary amine groups (398.5 eV), and the second and major component (399.9 eV) which could be attributed to either imines and secondary amines in the CHX formula or amides related to the plasma process. In the case of sample CHX-1, the low O/N ratio (cf. Table 1) indicates that this major component (399.9 eV) is mainly related to oxygen free moieties such as those in the biguanide structure, whereas for sample CHX-2 some contribution of surface amide groups generated after deposition cannot be discarded.

Deconvolution of the C1s peaks is relatively complex. The different components can be ascribed to: C–C/C–H (284.6 eV), C = N (285.6 eV), C–Cl (287 eV) and C = O (288.2 eV). In case of Cl2p peaks (Fig. 2(a)), we can identify two contributions: the organic chloride (~200 eV) and inorganic chloride (196.9 eV) peaks alongside to the corresponding spin-orbit splitting peaks shifted 1.6 eV.

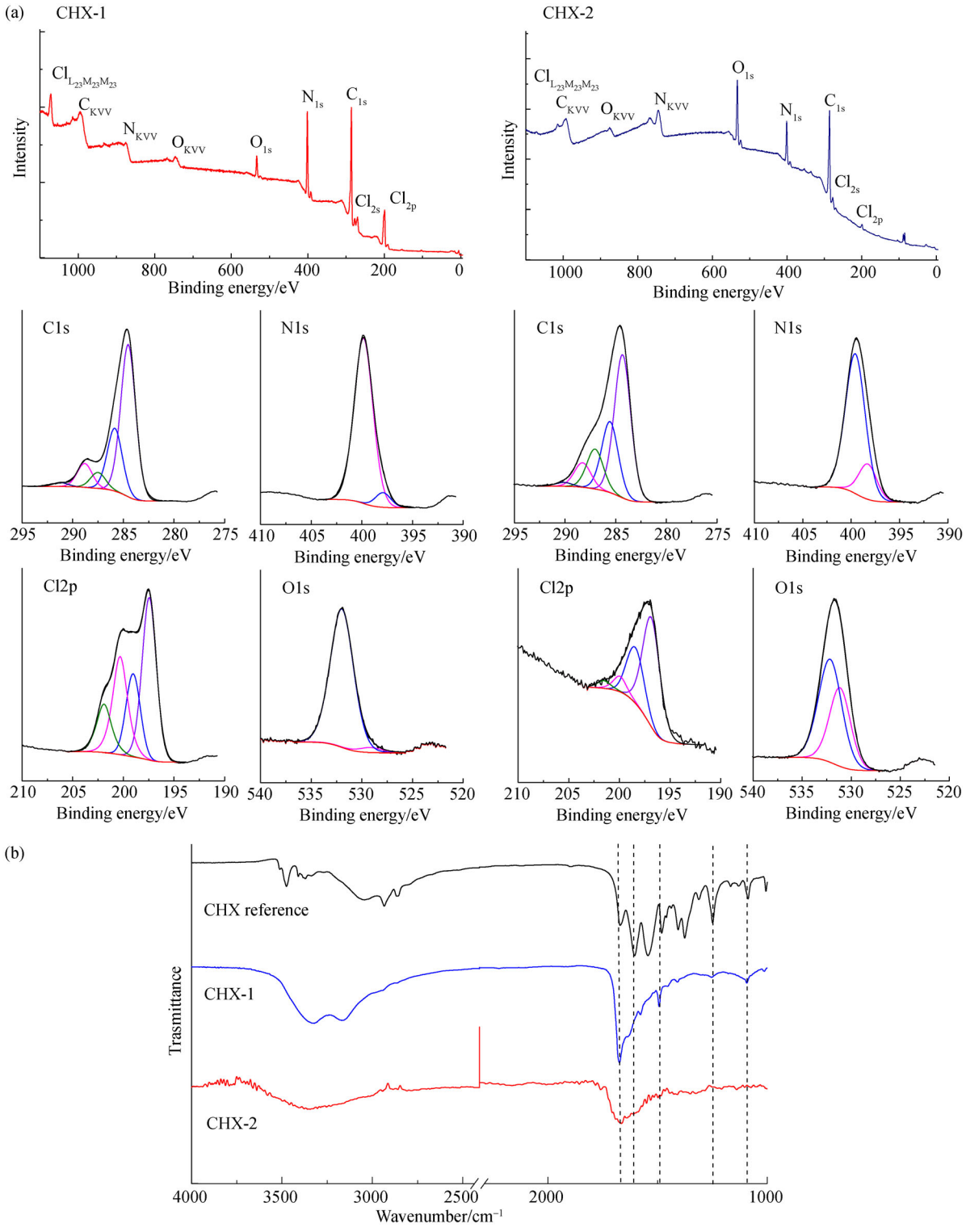

Fig. 2 (a) XPS Survey and C1s, N1s, Cl2p and O1s spectra of CHX-1 and CHX-2 films; (b) FT-IR spectra of a CHX reference precursor powder in KBr, CHX-1 and CHX-2 plasma nanocoatings. Grid lines mark the CHX main vibration bands preserved in the films

Table 1 Atomic composition of CHX-1 and CHX-2 plasma films and percentages corresponding to the CHX molecule excluding H content inaccessible by XPS

Sample	O1s /%	N1s /%	Cl2p /%	C1s /%
CHX molecule	–	29.4	5.9	64.7
CHX-1	4.2	24.7	11.2	59.9
CHX-2	17.4	16.6	1.2	64.8

Inorganic chloride groups in the surface of the thin films are very likely originated from the extensive plasma recombination and fragmentation processes of a percentage of the precursor molecules during the synthesis of RPAVD thin films.

The O1s (Fig. 2(a)) is adjusted with two overlapping components at 531.3 and 532.3 eV, which are related to C = O and C–O bonds, respectively, and to oxygen in H_2O and –OH groups. Therefore, it is difficult to discriminate the percentage of each specie by this technique.

The plasma films and a pristine CHX powder reference sample were analyzed by FT-IR and compared with those reported [43]. The corresponding spectra are shown in Fig. 2(b). The precursor powder spectrum presents a set of well-defined features in the range 3500–3200 cm^{-1}, which can be attributed to N–H stretching vibration of the different = NH and –NH groups in the biguanide structure, together with a broad band with a maximum at ~3050 cm^{-1} ascribed to the C–H stretching modes of the chloroaniline group. Other sharp peaks at 2935 and 2885 cm^{-1} correspond, respectively, to the asymmetric and symmetric C–H stretching modes of the central saturated chain. The most intense features of the CHX molecule appear in the range 1700–1500 cm^{-1}. Several studies relate these bands to biguanide vibrations in CHX but with dissimilar assignment [37,44–47]. In general, the larger frequency vibration at ~1670 cm^{-1} is attributed to C = N stretching, whereas the rest of features are related to vibration modes of C–N and N–H in biguanide and the C = C stretching in the chloroaniline ring. Other relevant characteristics identified in the CHX spectrum are the CH_2 deformation vibration at 1480 cm^{-1}, the coupling vibration δ(NH) + ν (C–N) at 1375 cm^{-1}, the Ar–N stretching at 1250 cm^{-1}, the Ar–Cl stretching in the para-substituted ring (1090 cm^{-1}), and the C–H out of plane vibration (810 cm^{-1}).

The infrared spectra of both RPAVD nanocoatings in Fig. 2(b) present intense features in the same region as the CHX molecules but show an important broadening and displacement in positions. Such structural features are expected for a cross-linked matrix consisting of large CHX fragments formed from the plasma interaction and eventually entire precursor molecules as it has been extensively reported for different plasma polymers [48] and RPAVD films grown from other functional precursor molecules [17–22]. During the deposition of the CHX-2 sample, the growing coating is exposed to a stronger plasma interaction due to the used geometrical arrangement (cf. experimental section). This explains the intense band-broadening of spectrum of CHX-2 in comparison to CHX-1. Thus, in the range 3500–3200 cm^{-1}, the well resolved NH stretching features of the powder spectrum turn into a broad band with a maximum at lower frequencies. Nonetheless, some contribution from-OH groups cannot be discarded in this region in the case of sample CHX-2 with a larger O content (cf. XPS data). A remarkable broadening is also apparent in the CHX features in the range 1700–1500 cm^{-1}. In this case, the plasma polymer spectra preserve an intense asymmetric band peaking at 1670 cm^{-1}. The maximum of this band matches with the C = N vibration of the biguanidine and some other low-frequency shoulders are attributed to C–N and N–H groups of this structure, indicating the retention of the guanidine structure during the RPAVD process. Similarly, the CH_2 deformation vibration and Ar–N stretching are also identified the IR spectra of the plasma coatings, particularly in case of sample CHX-1 synthetized under softer plasma conditions.

Surface wettability is a key property for any biomedical surface because it will determine the surface interactions with proteins and cells. Cell adhesion and proliferation are favored on hydrophilic surfaces because these type of surfaces promote the proper integration of a nanocoating under physiological conditions [3,26,27]. As indicated previously, the PDMS surface possess high hydrophobic nature with low biocompatibility. Thus, one of the key properties of our CHX nanocoatings on PDMS (CHX/PDMS) has to be an enduring hydrophilicity. The contact angle values and the corresponding surface energies from the CHX/PDMS plasma films and the PDMS substrates are gathered in Table 2. The results indicate the CHX-1/PDMS nanocoatings are superhydrophilic (WCA < 10°). The CHX-2/PDMS coatings also present a hydrophilic surface (WCA = 54°), which is very likely due to a higher cross-linking character. Besides, our results indicates these WCA values remain unaltered for at least six months after deposition for samples stored in air. Thus, the characteristic fast hydrophobic recovery typically observed in treated PDMS surfaces is effectively inhibited by the CHX nanocoatings.

Stability of the CHX/PDMS nanocoatings in the liquid culture medium (LB) used for growth of the *E. coli* was also analyzed by UV-VIS absorption spectroscopy after

Table 2 WCA and DCA values of CHX nanocoatings and their corresponding surface energy values

Sample	WCA /°	DCA /°	Surface energy /(mJ·m^{-2})
PDMS	112±2	78±2	9.5±4
CHX-1/PDMS	< 10	48±2	98±4
CHX-2/PDMS	54±2	38±3	111±4

10 min of immersion (Fig. 1(c)). The CHX-2/PDMS hydrophilic nanocoatings demonstrated a much better stability than superhydrophilic CHX-1/PDMS samples. In fact, the UV-VIS absorption spectrum of sample CHX-2 (Fig. 1(c))) was unaffected by the immersion test, whereas a partial loss of material is evidenced for sample CHX-1/PDMS. These different behaviors of the two CHX films in solution will modify their bactericidal properties as analyzed in the next section.

3.3 Antiseptic properties and biocompatibility

Antiseptic activity of CHX RPAVD nanocoatings on PDMS was investigated by agar diffusion method in contact with *E. coli* K12 strain used as microorganism model. The results are gathered in Fig. 3. Thus, for both types of RPAVD coatings bacterial growth was effectively inhibited in almost the entire surface of the samples as compared to uncoated PDMS foils used as negative control (Fig. 3(a)). The figure also discloses the different antibacterial action-mechanism of coatings CHX-1 and CHX-2. For CHX-2 samples, antibacterial activity is circumscribed to the surface of the RPAVD nanocoating. In this sample, a triangular zone colonized by *E. coli* (detail in Fig. 3(a)) can be observed and corresponds to a region without the RPAVD coating protected by a fixing clamp during the deposition. This points to a contact–based antibacterial mechanism (either contact killing or anti-adhesion processes). In contrast, CHX-1 samples produce a region of growth inhibition that extends out of the sample contact zone, clearly indicating the release of antiseptic agents from the RPAVD surface. The corresponding inhibition area can be determined from the analysis of the picture [49], obtaining a value of 3.5±0.1 mm. These differences together with the loss of material observed in solution for sample CHX-1 (i.e., the decreasing in light absorption in the UV region and the loss of the interference fringes of the CHX-1 film in solution shown in Fig. 1(c)) indicates that the antibacterial action of sample CHX-1 involves the release of biocidal agents. The biocide activity of the CHX-1 plasma coatings was investigated as a function of the coating thickness. Figure 3(b) shows the results corresponding to three CHX-1 samples with coating thickness of 150, 75 and 30 nm. The radius of the bacterial-inhibition zones gradually increases with the coating thickness. Thus, the inhibition areas estimated from the analysis of the pictures in Fig. 3(b) are: 2.1±0.2, 1.5±0.3 and 0.5±0.1 mm, for the 150, 75 and 30 mm samples, respectively. Even for ultrathin films of 30 nm, the culture-inhibition area is larger than the contact surface, in contrast with the CHX-2 samples. Besides, the antibacterial activity of the studied films remains for at least one week as no noticeable growth of the bacterial lawns was observed in any of the studied samples in this period.

Adhered bacteria after agar diffusion test were studied by FESEM microscopy. The micrographs in Fig. 4(a),

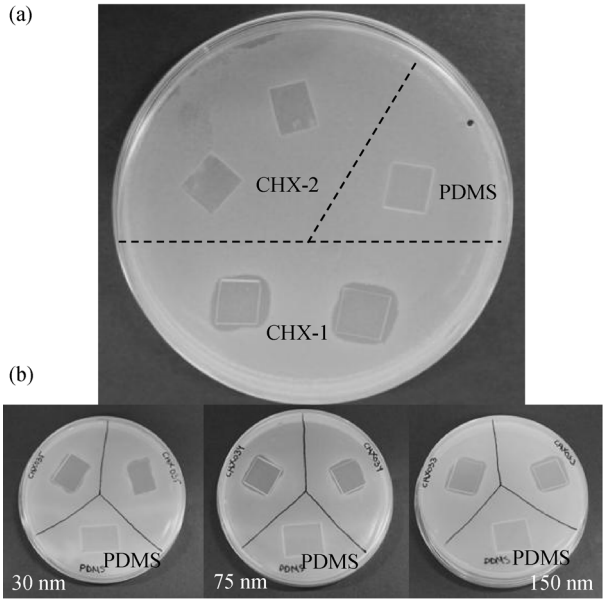

Fig. 3 (a) Result of agar diffusion test where bacteria growth inhibition by CHX-1 and CHX-2 nanocoatings can be observed and compared to an uncoated PDMS foil (negative control); (b) Agar diffusion test for CHX-1 nanocoating (top) as a function of the thickness in comparison to unmodified PDMS foil (bottom). The radius of inhibition increases with the thickness of the RPAVD film

show a total colonized surface of PDMS by *E. coli*, whereas in CHX-1 only isolated lysed-appearance bacteria and ruptured clusters could be found over the total sample surface. In case of CHX-2, bacteria colonization was only found in the uncoated area corresponding to the clamp position.

Bacteria viability over CHX surfaces was analyzed by

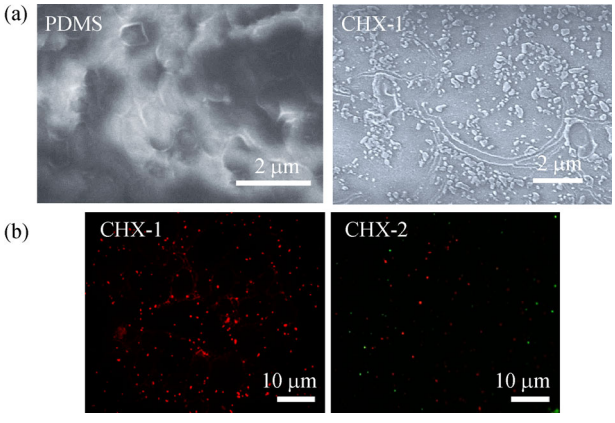

Fig. 4 (a) FESEM top-view micrographs of unmodified PDMS foil and CHX-1 nanocoating surfaces after agar diffusion test; (b) Fluorescence micrographs of live/dead bacteria for viability analysis of CHX-1 and CHX-2 antibacterial RPAVD coatings after agar diffusion test. Green signals indicate viable bacteria and red signals dead or damage cells

fluorescence microscopy. After agar diffusion test, the coatings were immersed into green emitting FDA and red emitting PI staining solutions to specifically tag living and dead bacteria, respectively. In this type of analysis, *E. coli* bacterial agglomerates over the studied surface becoming visible in the form of green (living bacteria) dots after dye. In comparison with control PDMS surfaces (not shown), the RPAVD antibacterial coatings CHX-1 and CHX-2 present a comparatively very much lower surface concentrations of microorganisms randomly distributed over the inspected surfaces, confirming their antibacterial activities. The differences between the two images in Fig. 4(b) provide insights into the antibacterial mechanisms operating in the two surfaces. First, no living bacteria (green dot) can be detected over sample CHX-1, agreeing with the strong biocidal character inferred from the agar diffusion test. On the other hand, dead organisms and a very minor concentration of living bacteria can be identified only over CHX-2 samples, indicating that their bactericidal efficiency is lower than that of the CHX-1 samples. However, the total amount of microorganims (both living and dead) is significantly lower on CHX-2 than on CHX-1. These results suggest that the plasma coatings have high antibacterial activity and the influence of additional antibacterial mechanism is very likely related to anti-adhesion processes.

Biocompatibility of RPAVD CHX films in terms of cell attachment and viability was assessed by culturing MG-63 human osteoblastic-line on both CHX-1 and CHX-2 nanocoatings. Cell adhesion over the samples was quantitatively analyzed after 24 h of incubation and results are displayed in Fig. 5, together with two different positive controls. For CHX-2 nanocoatings, cell viability values were around 90%. These values were not statically different with respect to both controls, proving the good biocompatibility of this RPAVD coating. In the case of CHX-1 nanocoating, cell viability decreased down to 60%. This result is very likely related to the release of biocide agents and the higher presence of biocide is responsible for the faster antiseptic response.

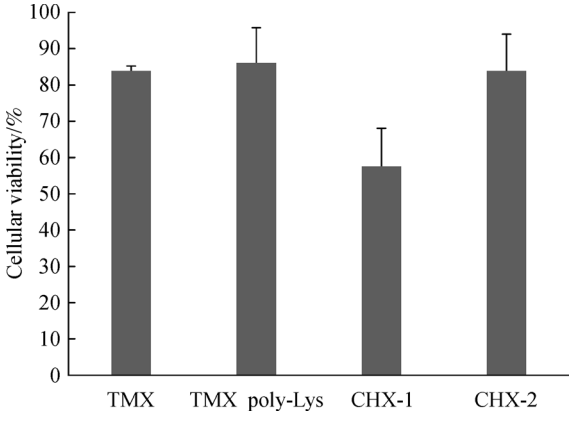

Fig. 5 Viability analysis of osteoblastic-like cells (cell line MG-63) over Thermanox® (TMX), TMX with poly-lysine coating (TMX poly-lys) control discs, and CHX-1 and CHX-2 RPAVD nanocoatings. No significant difference with respect to the control discs ($p < 0.05$) were observed

4 Conclusions

We have develop a novel type of antibacterial nanocoatings by remote plasma assisted vacuum deposition on PDMS from commercial clorhexidine powder at room temperature. The retention of biocide groups in the polymer matrix has been confirmed by XPS and FT-IR. Besides the antibacterial properties, the coatings also improve the biocompatibility of PDMS substrates, making their surfaces permanently hydrophilic. The plasma coatings act as an effective surface diffusion barriers for low weight hydrophobic PDMS moieties from the bulk. The coatings are transparent and cannot be perceived by visual inspection of the PDMS coated surfaces. Two different types of antibacterial coatings have been synthetized through the same process. The CHX-1 nanocoatings act as rapid biocide deliver whose effect depends on its thickness. The CHX-2 can be used as a localized contact based antibacterial coatings without the release of antiseptic agent to the local environment, extending the antiseptic activity temporal window. Because both approaches are based on the same synthesis route and antiseptic compound, they might be easily combined during a single fabrication run for the development of single, and gradient/multilayered bifunctional systems with characteristics adapted to a specific biomedical application (i.e., number and type of coatings and the thickness and extension of each layer), combining the inherent advantages each antibacterial mechanism. To the best of our knowledge, this is the first demonstration of biocidal nanocoatings based on direct commercial antiseptic deposition by plasma-enhanced deposition process. The RPAVD procedure is easily scaled up to large area industrial production and can be directly extended to other type of thermally stable antiseptic compounds for the development of a novel generation of advanced antiseptic coatings on biomedical substrates.

Acknowledgements We thank Ministerio de Economía y Competitividad of Spain, the Agencia Estatal de Investigación (AEI) and EU (FEDER program) under grant MAT2016-79866-R.

References

1. Cavallaro A A, Macgregor-Ramiasa M N, Vasilev K. Antibiofouling properties of plasma-deposited oxazoline-based thin films. ACS Applied Materials & Interfaces, 2016, 8(10): 6354–6362
2. Vähä-Nissi M, Pitkänen M, Salo E, Kenttä E, Tanskanen A, Sajavaara T, Putkonen M, Sievänen J, Sneck A, Rättö M, Karppinen

M, Harlin A. Antibacterial and barrier properties of oriented polymer films with ZnO thin films applied with atomic layer deposition at low temperatures. Thin Solid Films, 2014, 562: 331–337

3. Zhang B, Myers D, Wallace G, Brandt M, Choong P. Bioactive coatings for orthopaedic implants—recent trends in development of implant coatings. International Journal of Molecular Sciences, 2014, 15(7): 11878–11921
4. Banerjee I, Pangule R C, Kane R S. Antifouling coatings: Recent developments in the design of surfaces that prevent fouling by proteins, bacteria, and marine organisms. Advanced Materials, 2011, 23(6): 690–718
5. Gilabert-Porres J, Martí S, Calatayud L, Ramos V, Rosell A, Borrós S. Design of a nanostructured active surface against gram-positive and gram-negative bacteria through plasma activation and *in situ* silver reduction. ACS Applied Materials & Interfaces, 2016, 8(1): 64–73
6. Jiang F, Yeh C K, Wen J, Sun Y. N-Trimethylchitosan/alginate layer-by-layer self assembly coatings act as 'fungal repellents' to prevent biofilm formation on healthcare materials. Advanced Healthcare Materials, 2015, 4(3): 469–475
7. Li L, Pu T, Zhanel G, Zhao N, Ens W, Liu S. New biocide with both *n*-chloramine and quaternary ammonium moieties exerts enhanced bactericidal activity. Advanced Healthcare Materials, 2012, 1(5): 609–620
8. Wu M, He J, Ren X, Cai W S, Fang Y C, Feng X Z. Development of functional biointerfaces by surface modification of polydimethylsiloxane with bioactive chlorogenic acid. Colloids and Surfaces. B, Biointerfaces, 2014, 116: 700–706
9. Yu Q, Wu Z, Chen H. Dual-function antibacterial surfaces for biomedical applications. Acta Biomaterialia, 2015, 16: 1–13
10. Agarwal A, Nelson T B, Kierski P R, Schurr M J, Murphy C J, Czuprynski C J, McAnulty J F, Abbott N L. Polymeric multilayers that localize the release of chlorhexidine from biologic wound dressings. Biomaterials, 2012, 33(28): 6783–6792
11. He T, Zhang Y, Lai A C K, Chan V. Engineering bio-adhesive functions in an antimicrobial polymer multilayer. Biomedical Materials (Bristol, England), 2015, 10(1): 15015
12. Verraedt E, Braem A, Chaudhari A, Thevissen K, Adams E, Van Mellaert L, Cammue B P A, Duyck J, Anné J, Vleugels J, Martens J A. Controlled release of chlorhexidine antiseptic from microporous amorphous silica applied in open porosity of an implant surface. International Journal of Pharmaceutics, 2011, 419(1-2): 28–32
13. Yu Q, Ge W, Atewologun A, Stiff-Roberts A D, López G P. Antimicrobial and bacteria-releasing multifunctional surfaces: Oligo (*p*-phenylene-ethynylene)/poly (*N*-isopropylacrylamide) films deposited by RIR-MAPLE. Colloids and Surfaces. B, Biointerfaces, 2015, 126: 328–334
14. Chang C H, Yeh S Y, Lee B H, Hsu C W, Chen Y C, Chen C J, Lin T J, Chen M H C, Huang C T, Chen H Y. Compatibility balanced antibacterial modification based on vapor-deposited parylene coatings for biomaterials. Journal of Materials Chemistry. B, Materials for Biology and Medicine, 2014, 2(48): 8496–8503
15. Nikiforov A Y, Deng X, Onyshchenko I, Vujosevic D, Vuksanovic V, Cvelbar U, De Geyter N, Morent R, Leys C. Atmospheric pressure plasma deposition of antimicrobial coatings on non-woven textiles. European Physical Journal Applied Physics, 2016, 75(2): 24710
16. Ostrikov K, Levchenko I, Keidar M, Cvelbar U, Mariotti D, Mai-Prochnow A, Fang J. Novel biomaterials: Plasma-enabled nanostructures and functions. Journal of Physics. D, Applied Physics, 2016, 49(27): 273001
17. Barranco A, Groening P. Fluorescent plasma nanocomposite thin films containing nonaggregated rhodamine 6G laser dye molecules. Langmuir, 2006, 22(16): 6719–6722
18. Barranco A, Aparicio F, Yanguas-Gil A, Groening P, Cotrino J, González-Elipe A R. Optically active thin films deposited by plasma polymerization of dye molecules. Chemical Vapor Deposition, 2007, 13(6-7): 319–325
19. Aparicio F J, Holgado M, Borras A, Blaszczyk-Lezak I, Griol A, Barrios C A, Casquel R, Sanza F J, Sohlstrom H, Antelius M, González-Elipe A R, Barranco A. Transparent nanometric organic luminescent films as UV-active components in photonic structures. Advanced Materials, 2011, 23(6): 761–765
20. Aparicio F J, Alcaire M, González-Elipe A R, Barranco A, Holgado M, Casquel R, Sanza F J, Griol A, Bernier D, Dortu F, Cáceres S, Antelius M, Lapisa M, Sohlström H, Niklaus F. Dye-based photonic sensing systems. Sensors and Actuators. B, Chemical, 2016, 228: 649–657
21. Blaszczyk-Lezak I, Aparicio F J, Borrás A, Barranco A, Álvarez-Herrero A, Fernández-Rodríguez M, González-Elipe A R. Optically active luminescent perylene thin films deposited by plasma polymerization. Journal of Physical Chemistry C, 2009, 113(1): 431–438
22. Aparicio F J, Alcaire M, Borras A, Gonzalez J C, López-Arbeloa F, Blaszczyk-Lezak I, González-Elipe A R, Barranco A. Luminescent 3-hydroxyflavone nanocomposites with a tuneable refractive index for photonics and UV detection by plasma assisted vacuum deposition. Journal of Materials Chemistry. C, Materials for Optical and Electronic Devices, 2014, 2(32): 6561–6573
23. Sangamesh K, Laurencin C, Deng M, eds. Natural and Synthetic Biomedical Polymers. San Diego: Elsevier, 2014, 301–308
24. Chen H, Brook M A, Sheardown H. Silicone elastomers for reduced protein adsorption. Biomaterials, 2004, 25(12): 2273–2282
25. Thevenot P, Hu W, Tang L. Surface chemistry influences implant biocompatibility. Current Topics in Medicinal Chemistry, 2008, 8 (4): 270–280
26. Gilbert P, Allison D G, Brading M, Verran J, Walker J. Biofilm community interactions: Chance or necessity? Cardiff: Bioline, 2001, 11–22
27. Wilson C J, Clegg R E, Leavesley D I, Pearcy M J. Mediation of biomaterial-cell interactions by adsorbed proteins: A review. Tissue Engineering, 2005, 11(1-2): 1–18
28. Zhang H, Chiao M. Anti-fouling Coatings of poly(dimethylsiloxane) devices for biological and biomedical applications. Journal of Medical and Biological Engineering, 2014, 35(2): 143–155
29. Larson B J, Gillmor S D, Braun J M, Cruz-Barba L E, Savage D E, Denes F S, Lagally M G. Long-term reduction in poly(dimethylsiloxane) surface hydrophobicity via cold-plasma treatments. Langmuir, 2013, 29(42): 12990–12996
30. Forster S, McArthur S L. Stable low-fouling plasma polymer coatings on polydimethylsiloxane. Biomicrofluidics, 2012, 6(3):

036504

31. Lee D, Yang S. Surface modification of PDMS by atmospheric-pressure plasma-enhanced chemical vapor deposition and analysis of long-lasting surface hydrophilicity. Sensors and Actuators. B, Chemical, 2012, 162(1): 425–434
32. Kaelble D H. Dispersion-polar surface tension properties of organic solids. Journal of Adhesion, 1970, 2(2): 66–81
33. Owens D K, Wendt R C. Estimation of the surface free energy or polymers. Journal of Applied Polymer Science, 1969, 13(8): 1741–1747
34. Balouiri M, Sadiki M, Ibnsouda S K. Methods for *in vitro* evaluating antimicrobial activity: A review. Journal of Pharmaceutical Analysis, 2016, 6(2): 71–79
35. Mestieri L B, Gomes-Cornélio A L, Rodrigues E M, Faria G, Guerreiro-Tanomaru J M, Tanomaru-Filho M. Cytotoxicity and bioactivity of calcium silicate cements combined with niobium oxide in different cell lines. Brazilian Dental Journal, 2017, 28(1): 65–71
36. Aparicio F J, Borras A, Blaszczyk-Lezak I, Gröning P, Álvarez-Herrero A, Fernández-Rodríguez M, González-Elipe A R, Barranco A. Luminescent and optical properties of nanocomposite thin films deposited by remote plasma polymerization of Rhodamine 6G. Plasma Processes and Polymers, 2009, 6(1): 17–26
37. Aparicio F J, Blaszczyk-Lezak I, Sánchez-Valencia J R, Alcaire M, González J C, Serra C, González-Elipe A R, Barranco A. Plasma deposition of perylene-adamantane nanocomposite thin films for NO_2 room-temperature optical sensing. Journal of Physical Chemistry C, 2012, 116(15): 8731–8740
38. Beamson G, Briggs D. High Resolution XPS of Organic Polymers. New York: John Wiley & Sons Ltd., 1990, 277–287
39. Yim J H, Fleischman M S, Rodriguez-Santiago V, Piehler L T, Williams A A, Leadore J L, Pappas D D. Development of antimicrobial coatings by atmospheric pressure plasma using a guanidine-based precursor. ACS Applied Materials & Interfaces, 2013, 5(22): 11836–11843
40. Yook J Y, Lee M, Song K H, Jun J, Kwak S. Surface modification of poly(ethylene-2,6-naphthalate) using NH_3 plasma. Macromolecular Research, 2014, 22(5): 534–540
41. Aparicio F J, Thiry D, Laha P, Snyders R. Wide range control of the chemical composition and optical properties of propanethiol plasma polymer films by regulating the deposition temperature. Plasma Processes and Polymers, 2016, 13(8): 814–822
42. Jiang H, Grant J T, Enlow J, Su W, Bunning T J. Surface oxygen in plasma polymerized films. Journal of Materials Chemistry, 2009, 19 (15): 2234–2239
43. Sokrates G. Infrared and Raman Characteristic Group Frequencies: Tables and Charts. New York: Wiley-Interscience, 2001, 191–198
44. Kovtun A, Kozlova D, Ganesan K, Biewald C, Seipold N, Gaengler P, Arnold W H, Epple M. Chlorhexidine-loaded calcium phosphatenanoparticles for dental maintenance treatment: Combination of mineralising and antibacterial effects. RSC Advances, 2012, 2(3): 870–875
45. Badea M, Olar R, Iliş M, Georgescu R, Călinescu M. Synthesis, characterization, and thermal decomposition of new copper (II) complex compounds with chlorhexidine. Journal of Thermal Analysis and Calorimetry, 2012, 111(3): 1763–1770
46. Pal S, Tak Y K, Han E, Rangasamy S, Song J M. A multifunctional composite of an antibacterial higher-valent silver metallopharmaceutical and a potent wound healing polypeptide: A combined killing and healing approach to wound care. New Journal of Chemistry, 2014, 38(8): 3889–3898
47. Holešová S, Valášková M, Hlaváč D, Madejová J, Samlíková M, Tokarský J, Pazdziora E. Antibacterial kaolinite/urea/chlorhexidine nanocomposites: Experiment and molecular modelling. Applied Surface Science, 2014, 305: 783–791
48. Biederman H, ed. Plasma Polymer Films. London: Imperial College Press, 2004, 227–231
49. Labay C, Canal J M, Modic M, Cvelbar U, Quiles M, Armengol M, Arbos M A, Gil F J, Canal C. Antibiotic-loaded polypropylene surgical meshes with suitable biological behaviour by plasma functionalization and polymerization. Biomaterials, 2015, 71: 132–144